SUPPLEMENTAL MATERIAL

I. Model Derivation

We set up a mathematical model for sRNA-mediated regulation which is schematically depicted in Fig. 1A. Experimental studies indicated that heteroduplex association and dissociation proceed with rapid kinetics when compared to protein synthesis and degradation (1, 2). We therefore simplified the model by applying a rapid-equilibrium assumption as described in the following.

The differential equations of the model depicted in Fig. 1A read:

$$\begin{aligned} d[\text{Target}]/dt &= v_{syn,T} - k_{deg,T}\cdot[\text{Target}] - k_{on}\cdot[\text{Target}]\cdot[\text{sRNA}] + k_{off}\cdot[\text{Pair}] \\ d[\text{sRNA}]/dt &= v_{syn,S} - k_{deg,S}\cdot[\text{sRNA}] - k_{on}\cdot[\text{Target}]\cdot[\text{sRNA}] + k_{off}\cdot[\text{Pair}] \\ d[\text{Pair}]/dt &= k_{on}\cdot[\text{Target}]\cdot[\text{sRNA}] - k_{off}\cdot[\text{Pair}] - k_{deg,P}\cdot[\text{Pair}] \end{aligned} \quad (1)$$

Summing up these differential equations, and using the relationships $[T_{tot}] = [\text{Target}] + [\text{Pair}]$ and $[S_{tot}] = [\text{sRNA}] + [\text{Pair}]$ for the total amounts of target RNA and small RNA yields:

$$\begin{aligned} d[T_{tot}]/dt &= v_{syn,T} - k_{deg,T}\cdot([T_{tot}]-[\text{Pair}]) - k_{deg,P}\cdot[\text{Pair}] \\ d[S_{tot}]/dt &= v_{syn,S} - k_{deg,S}\cdot([S_{tot}]-[\text{Pair}]) - k_{deg,P}\cdot[\text{Pair}] \end{aligned} \quad (2)$$

The association/dissociation reactions of the pair are assumed to proceed much faster than all other steps in the model. Thus, the model species are related by the following equilibrium:

$$K_{d,P} = \frac{k_{off,P}}{k_{on,P}} = \frac{[\text{Target}]\cdot[\text{sRNA}]}{[\text{Pair}]} = \frac{([T_{tot}]-[\text{Pair}])\cdot([S_{tot}]-[\text{Pair}])}{[\text{Pair}]} \quad (3)$$

Solving for the pair concentration yields:

$$[\text{Pair}] = 1/2\cdot\left([T_{tot}]+[S_{tot}]+K_{d,P} - \sqrt{([T_{tot}]+[S_{tot}]+K_{d,P})^2 - 4\cdot[T_{tot}]\cdot[S_{tot}]}\right) \quad (4)$$

Equations (2) and (4) constitute a reduced form of the differential equation system (1) for the case that association/dissociation reactions of the pair proceed much faster than all other steps (‘rapid equilibrium approximation’). This reduced system was used for all numerical simulations shown in the main text and in the Supplement.

Analytical approximation for the subthreshold regime: The reduced differential equation system comprising Equations (2) and (4) was further simplified to derive an analytical expression for the response time in the subthreshold regime ($v_{syn,T} < v_{syn,S}$). Under subthreshold conditions, one can assume that the sRNA is present in vast excess over the target mRNA, so that $[S_{tot}]$ is approximately constant. Then, Eq. 4 for the Pair intermediate simplifies to

$$[\text{Pair}]=\frac{[T_{tot}]\cdot[S_{tot}]}{K_{d,P}+[S_{tot}]}, \quad (5)$$

and Eq. 2 reduces to

$$d[T_{tot}]/dt = v_{syn,T} - \left(k_{deg,T}\cdot\left(1-\frac{[S_{tot}]}{K_{d,P}+[S_{tot}]}\right) + k_{deg,P}\cdot\frac{[S_{tot}]}{K_{d,P}+[S_{tot}]}\right)\cdot[T_{tot}] \quad (6)$$

Thus, direct mRNA degradation and degradation via the Pair intermediate behave as two competing first-order decay terms in the subthreshold regime. For sufficiently large sRNA expression (i.e., $[S_{tot}] > K_{d,P}$) and/or if the degradation of the pair is faster than that of the monomeric mRNA ($k_{deg,P} > k_{deg,T}$) the system further simplifies to

$$d[T_{tot}]/dt = v_{syn,T} - k_{deg,P}\cdot[T_{tot}] \quad (7)$$

Thus, the response time t_{50} for mRNA up- and downregulation is proportional to the inverse of the degradation rate of the pair (3).

II. Kinetic Parameters Used for Modeling

This section summarizes the kinetic parameters used for the numerical simulations in Figs. 1 and 2. The synthesis of target RNA ($v_{syn,T}$) is modeled to be controlled by external stress stimuli (Fig. 1A). A simple change of the synthesis rate from one value to another was used in most simulations (Figs. 2A – D, S3B and S4B), while the Michaelis-Menten equation ($v_{syn,T} = V_{max,synT} \cdot$ Stimulus / ($K_{M,synT}$ + Stimulus)) was employed to simulate dose-response behavior (Figs. 1B, S3A, and S4A).

Table S1a

Figure	Fig. 1B	Fig. 2A	Fig. 2B
$v_{syn,T}$ [nM h^{-1}]	Modeled by Michaelis-Menten equation	247.2 (basal level) 1136 (after stimulus increase)	996.9 (basal level) 41.9 (after stimulus removal)
$V_{max,syn,T}$ [nM h^{-1}]	1.25	-	-
$K_{M,syn,T}$ [nM]	1	-	-
$k_{deg,T}$ [h^{-1}]	1	0.42	0.42
$v_{syn,S}$ [nM h^{-1}]	0.625	516.6 (solid line) 706.9 (grey line) 145.3 (dashed line)	516.6 (solid line) 145.3 (dashed line)
$k_{deg,S}$ [h^{-1}]	1	0.35	0.35
$K_{D,P}$ [nM]	0.001	0.0045	0.0045
$k_{deg,P}$ [h^{-1}]	10	13.75	13.75

Table S1b

Figure	Fig. 2C	Fig. 2D	Fig. S3A
$v_{syn,T}$ [nM h^{-1}]	0 (basal level) 1136 (after stimulus increase)	0 (basal level) 1136 (after stimulus increase)	Modeled by Michaelis-Menten equation
$V_{max,syn,T}$ [nM h^{-1}]	-	-	1.25
$K_{M,syn,T}$ [nM]	-	-	1
$k_{deg,T}$ [h^{-1}]	0.42	0.42	1
$v_{syn,S}$ [nM h^{-1}]	516.6 (solid line) 0 (dashed line)	516.6 (solid line) 0 (dashed line)	0.625
$k_{deg,S}$ [h^{-1}]	0.35	0.35	1
$K_{D,P}$ [nM]	0.0045	0.0045	0.001
$k_{deg,P}$ [h^{-1}]	13.75	13.75	1

Table S1c

Figure	Fig. S3B	Fig. S4A	Fig. S4B
$v_{syn,T}$ [nM h^{-1}]	0 (basal level) 1.25 (after stimulus increase)	Modeled by Michaelis-Menten equation	0 (basal level) 5 (after stimulus increase)
$V_{max,syn,T}$ [nM h^{-1}]	-	5	-
$K_{M,syn,T}$ [nM]	-	7	-
$k_{deg,T}$ [h^{-1}]	1	1	1
$v_{syn,S}$ [nM h^{-1}]	0.625	0.625	0.625
$k_{deg,S}$ [h^{-1}]	1	1	1
$K_{D,P}$ [nM]	0.001	0.001	0.001
$k_{deg,P}$ [h^{-1}]	1	10	10

III. Half-life measurements

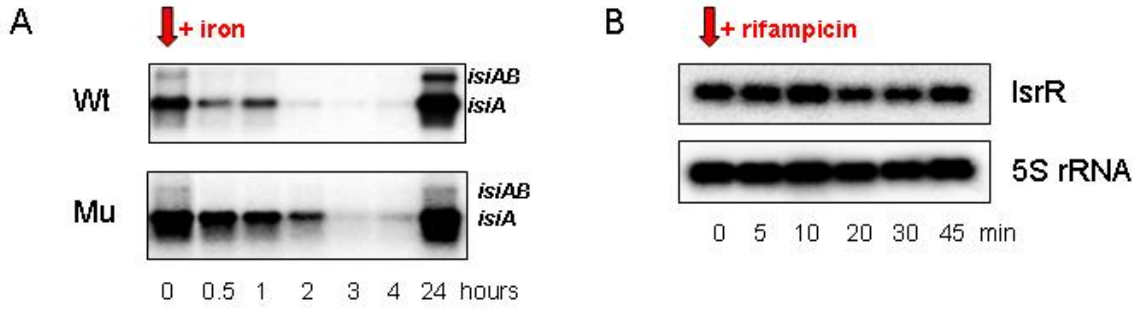

Figure S1: Degradation of transcripts from the *isiAB* operon. (A) Wildtype (Wt) and mutant (Mu) cells lacking the antisense RNA, IsrR, were cultivated under iron-deplete conditions. At time zero (0 hours) an iron pulse was given (red arrow), and cells were grown further for 0–24 hours. The *isiAB* dicistronic precursor transcript and the *isiA* mRNA are degraded directly after iron induction (0-4 hours), whereby the degradation rate of *isiA* mRNA is higher for Wt cells expressing the antisense RNA in comparison to the Mu cells lacking IsrR. (B) Cells were grown under iron-replete conditions. Although at time zero (0 min) rifampicin was added to non-specifically arrest transcription, accumulation of IsrR transcripts is not affected compared to an internal standard (5S rRNA) for at least 45 min, thus indicating a half-life > 45 min for IsrR. The RNA transcripts were separated on 1.3% formaldehyde-agarose gels and hybridized with an RNA-specific DNA fragment.

IV. Dose-Response Measurements

Figure 1B and additional numerical simulations indicated that sRNAs might establish sharp thresholds in gene expression (compare (4)). These thresholds are typically accompanied by a mutually exclusive expression pattern of sRNA and target mRNA at least if the pair intermediate is significantly less stable than the monomeric RNAs. Our previous experimental work revealed that the mRNA of the cyanobacterial iron stress protein, *isiA*, and its modulator, the IsrR sRNA, are expressed in mutually exclusive manner under various stimulation conditions (5). Moreover, a comparison of wild-type cells with IsrR knockdown cells revealed that IsrR completely suppresses residual *isiA* expression under unstressed conditions (compare circle and square at t = 0 in Fig. 2A). These data suggest that a sharp threshold exists in the cyanobacterial iron stress response.

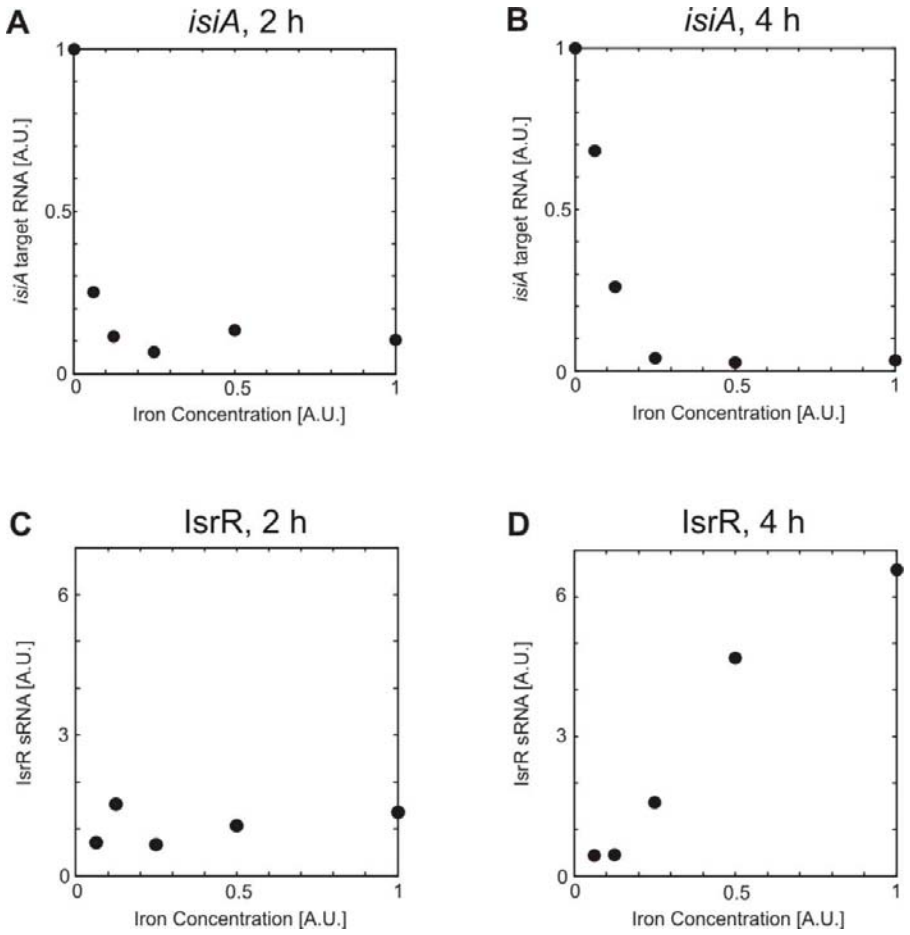

Figure S2: Dose-Response Behavior of the cyanobacterial iron stress response. Cells were cultivated under iron-starving conditions for 48 h to induce *isiA* expression, and then treated with different doses of iron to induce downregulation of *isiA* transcription. The expression levels of the *isiA* target RNA (A and B) or of the IsrR sRNA (C and D) were measured after 2h (A and C) and after 4 h (B and D).

We performed dose-response experiments to further confirm the existence of such thresholds. Cells were cultivated under iron-starving conditions for 48 h to induce *isiA* expression, and then treated with different doses of iron to induce downregulation of *isiA* transcription. The corresponding measurements of *isiA* target RNA and IsrR sRNA (shown in Fig. S2) reveal that IsrR does not accumulate unless the *isiA* concentration falls a critical level (~0.05 in A and B). This conclusion holds in the time

domain and in the concentration domain. First, the *isiA* level 2 h after iron re-addition (Fig. S2A) is higher when compared to 4 h after iron re-addition (Fig. S2B), and accordingly IsrR expression is selectively induced at 4 h (Fig. S2C and D). Second, IsrR expression at 4h requires that the iron level exceeds a certain threshold (of approximately 0.25 in Fig. S2B and D). Taken together, these data indicate that a sharp threshold exists in the cyanobacterial iron stress response, and that the system operates near this threshold under physiological conditions.

V. Supplemental Numerical Simulations

Competition-only Model

In the main text, we mainly focused on the scenario, where the heteroduplex is much less stable than the target RNA. In this case, the sRNA plays a dual role in target RNA regulation, as it competitively inhibits translation and additionally induces RNA degradation. However, several prokaryotic and eukaryotic non-coding RNAs merely act as competitive inhibitors of translation, but do not affect target RNA degradation (6-8). In the following, we therefore analyze a "competition-only model", where the target RNA and the pair heteroduplex are degraded with the same rate constant (see Table S1 for kinetic parameters).

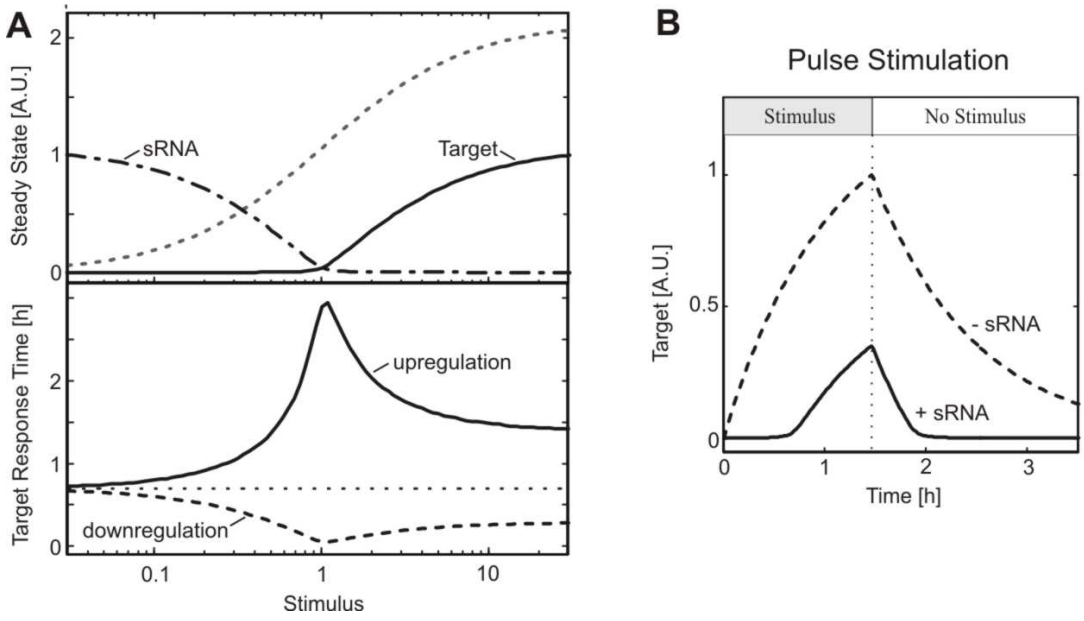

Figure S3: System behavior in case that the sRNA competitively inhibits translation, but does not enhance target degradation ("competition-only model"). **(A)** Steady State (top) and Dynamical (bottom) Response to Varying Stimulus Strength similar to Fig. 1B. The steady state dose-response and the response time were calculated for the *free* sRNA, while the response times in Fig. 1B were calculated for the total RNAs (i.e., the sum of free RNA and pair). See Supplemental Table S1 for kinetic parameters. **(B)** Time course of *free* target RNA in response to step-like pulse stimulation similar to Fig. 2C. See Supplemental Table S1 for kinetic parameters.

Figure S3 shows numerical simulations similar to those in Figs. 1B and 2C. It turned out that the competition-only model also shows the kinetic features discussed in the main text when analyzed at the level of *free* sRNA and *free* target RNA (Fig. S3). However, these features were no longer observed at the level of *total* sRNA and *total* target RNA (i.e., the sum of free and pair species), as pair formation does not induce RNA degradation, but only sequestration. For example, the *free* RNAs occur in a mutually exclusive manner in the competition-only model, while the *total* levels of target RNA and sRNA show overlapping expression patterns (not shown).

Partial-Degradation Model

In the default model, we assumed that both, the sRNA and target RNA, are degraded during the decay reaction of the pair heteroduplex. Eukaryotic miRNAs frequently remain intact after target degradation, and can guide the recognition and destruction of additional messages (7). We therefore extended the default model such that it takes such a more catalytic mode of action into account ('partial-degradation model'). The differential equations of the partial-degradation model are given by:

$$\begin{aligned} d[T_{tot}]/dt &= v_{syn,T} - k_{deg,T} \cdot ([T_{tot}]-[Pair]) - k_{deg,P} \cdot [Pair] \\ d[S_{tot}]/dt &= v_{syn,S} - k_{deg,S} \cdot ([S_{tot}]-[Pair]) - (1-f) \cdot k_{deg,P} \cdot [Pair] \end{aligned} \quad (8)$$

where the concentration of the pair is still given by Eq. (4). The new parameter f specifies the fraction of the sRNA that remains intact during the decay of the pair heteroduplex. For f = 0, the system reduces to the default model (Eq. (2)), while the sRNA is not degraded via the pair intermediate in case that f = 1.

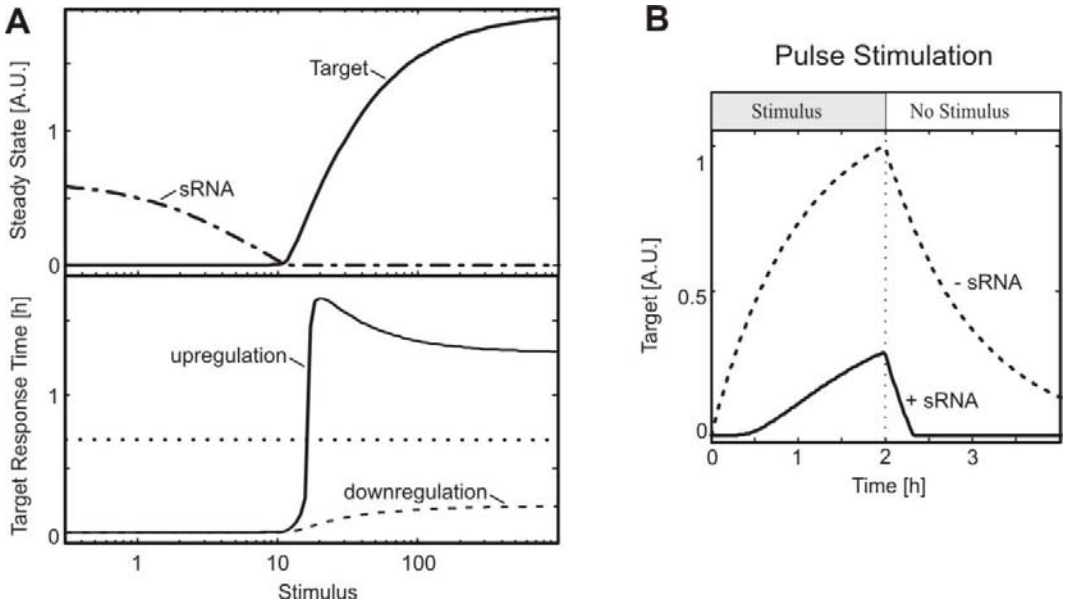

Figure S4: System Behavior in case that the sRNA remains intact during pair degradation ("partial-degradation model"). The simulations were done by integrating the extended differential equation system (8) and f was set to 0.8. **(A)** Steady State (top) and Dynamical (bottom) Response to Varying Stimulus Strength similar to Fig. 1B. See Supplemental Table S1 for kinetic parameters. **(B)** Time course of *free* target RNA in response to step-like pulse stimulation similar to Fig. 2C. See Supplemental Table S1 for kinetic parameters.

Figure S4 shows simulation results for f = 0.8 (i.e., 80% of the sRNA remains intact during pair degradation). The kinetic characteristics reported in the main text are still observed, and thus apply for eukaryotic miRNAs as well. Note that the threshold in Fig. S4A is shifted to higher values when compared to Fig. 1B, as expected ($v_{syn,T}$ has the same value for a stimulus of 1 in both simulations; compare Table S1).

VI. Simulation of pulse-filtering at the protein level

The analysis presented in the paper suggests that ultrasensitive pulse-filtering occurs at the mRNA level. However, it remained to be determined whether pulse-filtering is preserved at the level of protein expression. The differential equation system given in Eq. 2 was therefore modified, so that it takes by protein synthesis and degradation into account:

$$\begin{aligned} d[T_{tot}]/dt &= v_{syn,T} - k_{deg,T} \cdot ([T_{tot}]-[Pair]) - k_{deg,P} \cdot [Pair] \\ d[S_{tot}]/dt &= v_{syn,S} - k_{deg,S} \cdot ([S_{tot}]-[Pair]) - k_{deg,P} \cdot [Pair] \\ d[Protein]/dt &= k_{syn,Protein} \cdot ([T_{tot}]-[Pair]) - k_{deg,Protein} \cdot [Protein] \end{aligned} \quad (9)$$

Equation 9, together with Eq. 4, constitutes a model for sRNA-mediated regulation of protein expression, which was analyzed by numerical simulations. Duration-response curves were calculated and the maximum of the protein time course was taken as the response. Figure S5 shows the protein time course amplitude as a function of the stimulus pulse duration (normalized by the half-maximal pulse duration). The duration-response curve was calculated for different protein half-lives as indicated in the legend of Fig. S5, and the protein synthesis rate was taken to be $k_{syn,Protein} = k_{deg,Protein}$ to ensure the same steady state protein level is achieved regardless of the degradation rate chosen.

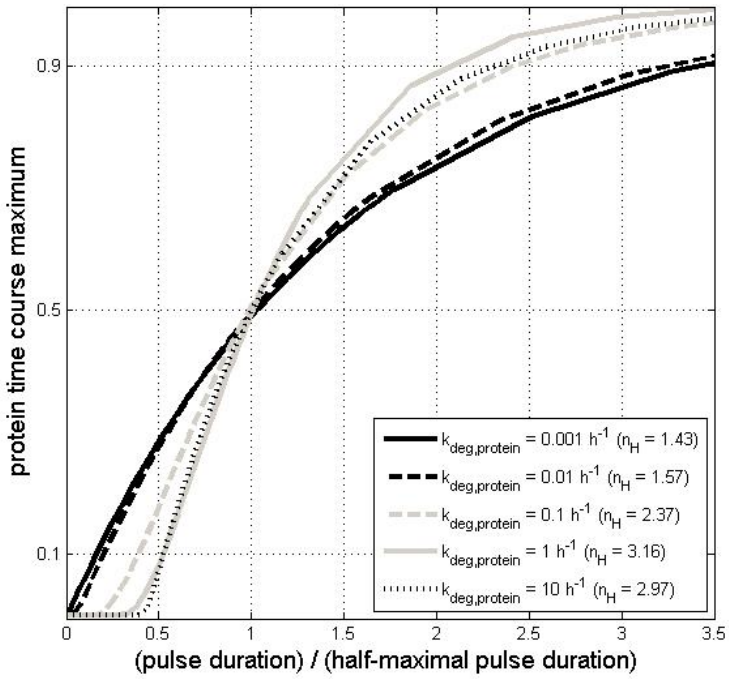

Figure S5: Pulse filtering is preserved at the protein level. The time course maximum of protein accumulation in response to step-like stimuli of different duration (but of constant strength) was simulated using the differential equation system (9). The duration-response curve was calculated for different protein half-lives as indicated in the legend, and the protein synthesis rate was taken to be $k_{syn,Protein} = k_{deg,Protein}$ to ensure the same steady state protein level is achieved regardless of the degradation rate chosen. All other kinetic parameters were chosen as in Fig. 2D. The x-axis was normalized by the pulse duration required to reach the half-maximal protein amplitude to allow for comparison among duration-response curves. The Hill coefficient of each curve was calculated as described in the Materials and Methods section, and is indicated in the legend.

The simulations in Fig. S5 demonstrate that pulse-filtering at the mRNA level (solid line in Fig. 2D) is obscured at the protein level if the protein half-life is 100 or 1000 hours (solid and dashed black lines). However, pulse-filtering is preserved at the protein level even if the protein has a half-life of 10 hours (Fig. S5, dashed grey line). The corresponding Hill coefficient of 2.37 implies that a ~6-fold change in the pulse duration is sufficient to switch the time course from 10% to 90% of the steady state activation level, and thus indicates ultrasensitive pulse filtering. More importantly, our simulations demonstrate that a system with 10 hour protein half-life completely filters out short pulse durations (Fig. S5, dashed grey line). As may be expected, pulse filtering is more pronounced for even shorter protein half-lives (grey solid and black dashed lines in Fig. S5), and ultrasensitivity at the protein and mRNA levels is similar (compare black solid line in Fig. 2D).

Degradation studies for the IsiA protein are missing in the literature so far. However, half-life measurements of the CP43 photosynthesis protein homologous to IsiA revealed a half-life of about an hour under stress conditions (9), and a similar rapid turnover was also reported for another photosynthesis protein, D1 (10). These data suggest that IsiA protein is short-lived in the experimental setup we have chosen, and that the pulse filtering property discussed here for the RNA level is observed at the level of proteins as well.

VII. Supplemental References

1. Wagner, E. G., S. Altuvia, and P. Romby. 2002. Antisense RNAs in bacteria and their genetic elements. Adv Genet 46:361-398.
2. Argaman, L., and S. Altuvia. 2000. fhlA repression by OxyS RNA: kissing complex formation at two sites results in a stable antisense-target RNA complex. J Mol Biol 300:1101-1112.
3. Hargrove, J. L., M. G. Hulsey, and E. G. Beale. 1991. The kinetics of mammalian gene expression. Bioessays 13:667-674.
4. Levine, E., Z. Zhang, T. Kuhlman, and T. Hwa. 2007. Quantitative characteristics of gene regulation by small RNA. PLoS Biol 5:e229.
5. Dühring, U., I. M. Axmann, W. R. Hess, and A. Wilde. 2006. An internal antisense RNA regulates expression of the photosynthesis gene isiA. Proc Natl Acad Sci U S A 103:7054-7058.
6. Morita, T., Y. Mochizuki, and H. Aiba. 2006. Translational repression is sufficient for gene silencing by bacterial small noncoding RNAs in the absence of mRNA destruction. Proc Natl Acad Sci U S A 103:4858-4863.
7. Bartel, D. P. 2004. MicroRNAs: genomics, biogenesis, mechanism, and function. Cell 116:281-297.
8. Urban, J. H., and J. Vogel. 2007. Translational control and target recognition by Escherichia coli small RNAs in vivo. Nucleic Acids Res 35:1018-1037.
9. Eichacker, L., H. Paulsen, and W. Rudiger. 1992. Synthesis of chlorophyll a regulates translation of chlorophyll a apoproteins P700, CP47, CP43 and D2 in barley etioplasts. Eur J Biochem 205:17-24.
10. Li, H., and L. A. Sherman. 2000. A redox-responsive regulator of photosynthesis gene expression in the cyanobacterium Synechocystis sp. Strain PCC 6803. J Bacteriol 182:4268-4277.